Incident IR Bandwidth Effects on Efficiency and Shaping for Third Harmonic Generation of Quasi-Rectangular UV Longitudinal Profiles[*]

Paul R. Bolton and Cecile Limborg-Deprey,
Stanford Linear Accelerator Center, MS-18,
2575 Sandhill Road, Menlo Park, California 94025

I. Introduction

The photocathode of the proposed LCLS RF Photoinjector will be irradiated by uv laser light which is generated as the third harmonic of incident fundamental ir laser light. We have investigated quantitatively the effect of input ir spectral bandwidth on the exiting longitudinal intensity profiles, energy conversion efficiencies and spectral bandwidths that characterize the third harmonic generation (THG) process with a pair of crystals. These profiles, efficiencies and bandwidths include the residual fundamental and residual second harmonic light exiting the second crystal. The intrinsic acceptance bandwidth for THG is determined by crystal material and thickness as well as the type of phase matching that is used. For our case of BBO material with type I phase matching these bandwidths are approximately 0.9 nm*cm and 0.1 nm*cm for second and third harmonic generation respectively. Consequently for fixed crystal thicknesses and a fixed input ir longitudinal profile, the specified input ir bandwidth will determine the profiles, efficiencies and bandwidths exiting the second crystal.

The results reported here are predictions of the SNLO code that is available as 'freeware' from the Sandia National Laboratories [1]. It has been modified for this work. It is critical to note that this modification has enabled us to generate SNLO predictions of the 'coupled' case in which the output of the first crystal is used as input to the second crystal. Our focus is the dependence of uv longitudinal intensity profile and THG efficiency on the input ir bandwidth and crystal thicknesses. We include here cases that best illustrate input bandwidth effects. The criteria for selection of reported cases are highest efficiency generation of quasi-rectangular uv profiles with proportional intensity ripple less than 5% rms on the plateau of the pulse. Maximizing THG efficiency typically amounts to maximizing the crystal thicknesses with the longitudinal profile constraint.

The specified incident ir longitudinal profile is quasi-rectangular (i.e. nonzero risetime and falltime with small intensity variation on the plateau) with a 10 psec pulse duration (FWHM). By assumption, this profile has been established upstream of the crystals at the fundamental ir wavelength. The simplest possible optical configuration is used in this work as shown in figure 1. The first crystal is the site of second harmonic generation (SHG) driven by the incident ir irradiation of central wavelength, 800nm. Downstream of the first crystal, the second crystal is the site of third harmonic generation (THG) which occurs by sum frequency mixing.

Inter-crystal optics (such as a half waveplate) are assumed to be lossless at the fundamental and second harmonic wavelengths. As shown in figure 1, a portion of the incident ir irradiation is not sequestered from the first crystal for subsequent THG in the second crystal. Also, quasi-phase matching configurations and other complex compensation schemes have not been investigated at this point. The simplistic geometry better elucidates the intrinsic acceptance bandwidth limitations imposed by the crystals.

Our goal in this endeavor has been to conduct a quantitative assessment of incident ir bandwidth effects on the THG process for BBO material of varied thicknesses and not, at this stage, to comply with all uv pulse specifications for the LCLS RF Photoinjector. Nonetheless, our results can be compared with LCLS photoinjector uv pulse requirements which call for a nominal 10 psec FWHM with 1 psec risetime and falltime and a nominally flat plateau (allowing for slope adjustments) with no more than a 5% rms proportional intensity variation. Furthermore, the results of this work can be used to suggest crystal thicknesses that would likely comply with all uv pulse requirements given the appropriate longitudinal profile and bandwidth for an input ir pulse.
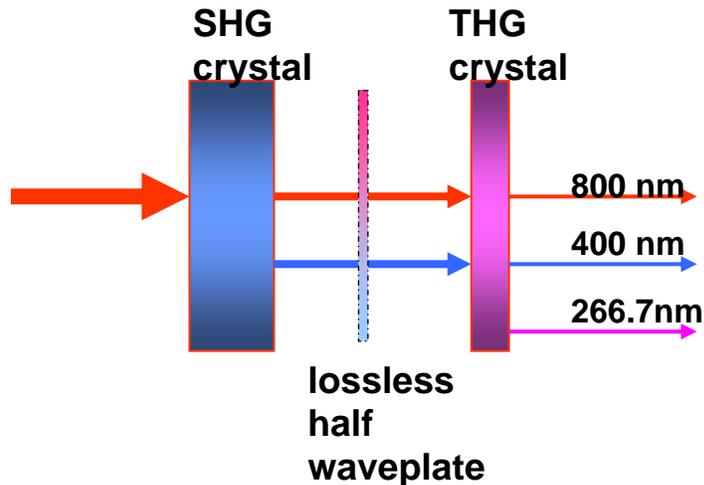
Figure 1. Simple optical configuration for THG

II. Methodology

The 800 nm ir pulse that is incident on the first crystal has a Gaussian transverse spatial profile with a spotsize, w of 3.4 mm (FWHM of 4.0 mm). The incident ir pulse energy is 20 mJ which corresponds to a peak intensity of 10 GW/cm^2 and a peak fluence of 110 mJ/cm^2 on the first BBO crystal. This fluence level is below estimated fluence thresholds for crystal surface and bulk damage [2,3]. No transverse profile shaping is implemented here (it is assumed that any transverse profile shaping would be implemented at the third harmonic wavelength downstream of the crystals and therefore decoupled from harmonic generation). The longitudinal plateau duration is defined to be the FWHM minus sixty percent of sum of the risetime and falltime. The risetime segment is illustrated in figure 2. This is intended to compensate for the 10% to 90% definition of the risetime and falltime. This means that the incident ir intensity plateau is the central

8.7 psec of the pulse duration where the FWHM is 10.0 psec and the risetime and falltime are 1.1 psec as shown in figure 3. The plateau region is flat as illustrated in figure 3.
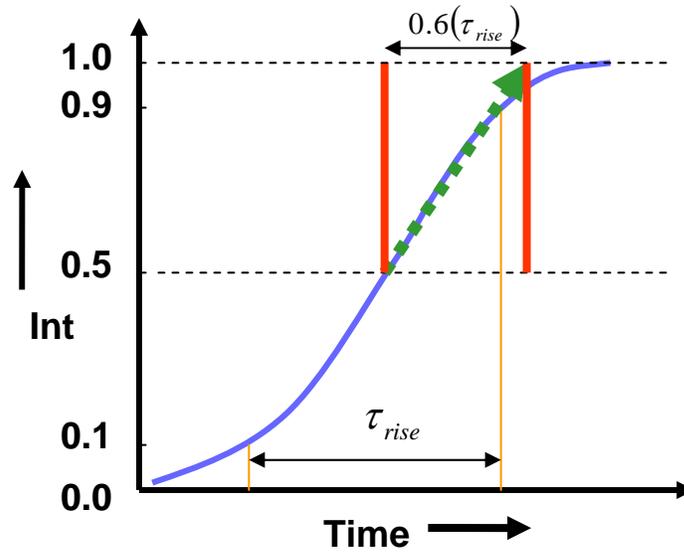
Figure 2. Risetime component of plateau definition
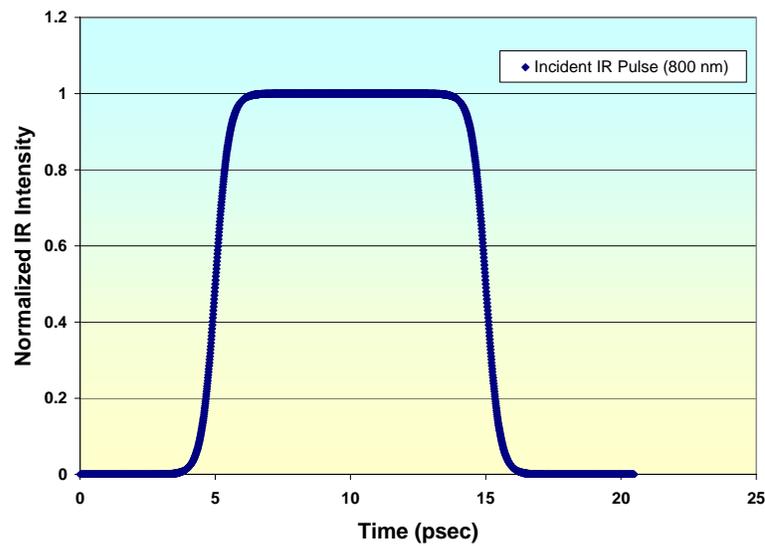
Figure 3. Incident normalized longitudinal ir intensity profile.

Dr. Arlee Smith has modified the short pulse plane-wave module of SNLO (PW-mix-SP) for this work to enable treatment of the coupled case for which longitudinal field amplitude profile and frequency modulation (chirp) data can be entered as a separate input file [1,4]. Because focusing effects are not included in these predictions, the 3.4 mm incident spotsize (radius) is fixed. Perfect type I phase matching is specified [5]. For type I phase matching in BBO, the group velocity mismatch for SHG is about 2% of c (the speed of light in vacuum) and for the THG process it is about 7% of c. This amounts to about 67 fsec of temporal walk off per millimeter of BBO crystal thickness for SHG and about 230 fsec of temporal walk off per millimeter of BBO for THG. That these estimates are significantly less than the risetime and falltime of these pulses is an advantage for longer pulses in general. In terms of physical lengths, the longitudinal walk off distance dominates the transverse birefringent walk off distance for a given crystal thickness, typically exceeding it by an order of magnitude or more. A linear absorption coefficient of 0.0015 cm^{-1} is used for the 800 nm wavelength and for 400 nm and 266.7 nm we used 0.02 cm^{-1}. An estimated value of 10^{-11} cm/W is used for the two-photon absorption coefficient for all three wavelengths. A nonlinear refractive index coefficient value of 8x10^{-16} cm^2/W is used. We also assume a 5 % reflectance at each crystal face (approximately equivalent to an uncoated optic). There is no pulse energy loss between the two crystals. All SNLO predictions apply to the exit face of the second crystal.

Given the above specified parameters, we have varied the spectral bandwidth of the incident ir pulse and also the thicknesses of each crystal for the given bandwidth. We have used incident ir spectral bandwidths of 2.5 nm (1.2 THz), 5.0 nm (2.3 THz), and 10.0 nm (4.7 THz) which have all been specified as a simple linear frequency chirp (i.e. a quadratic phase variation). Given the intrinsic acceptance bandwidths in BBO for type I SHG and THG processes, we anticipate optimum BBO crystal thicknesses to be less than 1mm.

III. Discussion of Results:

Tables I, II and III present best results for the bandwidth cases investigated**.** The following uv intensity profile parameters are included in the tables: full width at half of the maximum intensity (FWHM), the average of risetime and falltime, uv plateau duration, and rms ripple on the defined plateau. We also include the spectral bandwidth (FWHM) and the net energy conversion efficiency for the fundamental, second harmonic and third harmonic wavelengths. Note that the net conversion efficiencies listed in the table are at the exit face of the second crystal and are relative to the 20 mJ of ir incident on the first crystal. These energy ratios necessarily include all processes that contribute to the net energy content at a given wavelength. The following discussion of these results focuses on the third harmonic.

III (a) - 10 nm Incident ir Case:

Figure 4 illustrates typical longitudinal profiles that exit the first BBO crystal following the SHG process and that are to be combined in the second crystal for THG. The incident 10 nm ir bandwidth is less than the intrinsic acceptance value (for SHG) of 18 nm for this crystal thickness of 0.5 mm. For the SNLO code, the intrinsic acceptance bandwidth is defined to be the bandwidth over which the magnitude of the phase mismatch parameter, $\dfrac{L\Delta k}{2\pi}$ is less than or equal to 0.5. It exceeds (by about 13 %) the FWHM for the weak-coupling (low intensity) case for which there is insignificant pump depletion. An observable variation of the SHG efficiency is expected over a 10 nm bandwidth. Consequently, there is a clear central dip in the ir profile and a centrally peaked second harmonic profile with risetime and falltime much greater than the incident ir values. This profile distinction between the residual fundamental and second harmonic exiting the first crystal is enhanced with increasing BBO thickness beyond 0.5 mm. Table I lists best result THG cases. The profiles shown in figure 4 are typical of all the incident profiles relevant to this table.

Figure 5 reveals plots of normalized uv profiles for the three best cases of Table I. The highest THG efficiency of 4.5 % is obtained from the combination of 0.5 mm and 0.1 mm for the first and second BBO crystal respectively. The central dip for the case where the first crystal thickness is 0.6 mm is due to the increased SHG efficiency in the thicker first crystal. This dip is eliminated (filled in) with increasing second crystal thickness but at the cost of increased risetime and falltime, with reduced plateau duration, reduced acceptance bandwidth and likely reduced THG efficiency. In Table I, the maximum listed rms intensity variation in the plateau is only 3.5 % (for the first and second crystal thickness combination of 0.5 mm and 0.1 mm respectively).

The limitation on THG efficiency is imposed by the intrinsic acceptance bandwidth of the second BBO crystal which is equal to the incident ir value of 10 nm for a 0.1 mm thickness. Because the THG efficiency is quite low in all Table I cases, the ir and second harmonic longitudinal profiles exiting the second BBO crystal closely resemble those incident on this crystal.
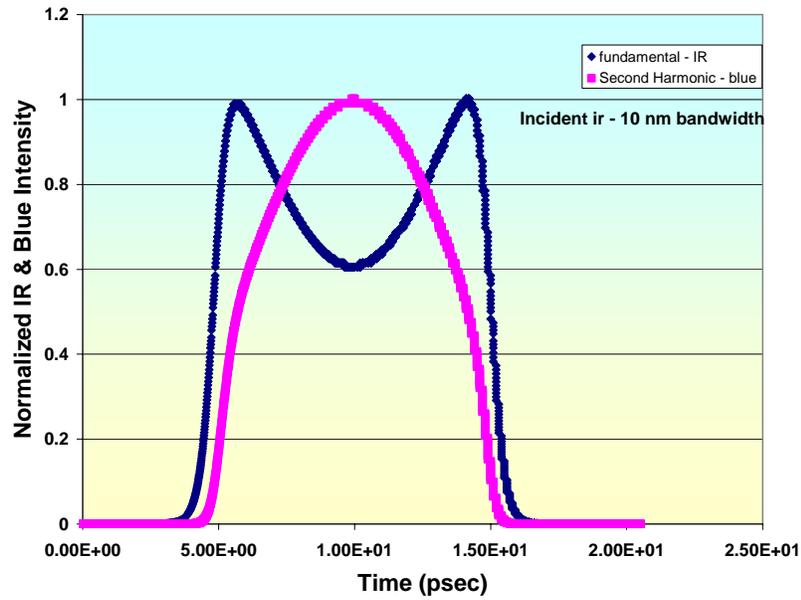
Figure 4. Normalized longitudinal intensity profiles of the fundamental and second harmonic pulses at the exit of the first (SHG) BBO crystal of 0.5 mm thickness for the 10 nm incident ir case

Table I: 10 nm bandwidth Case

		0.4	0.5	0.5	0.6	0.6
Crystal 1 depth (mm)		0.4	0.5	0.5	0.6	0.6
Crystal 2 depth (mm)		0.05	0.05	0.1	0.05	0.1
FWHM (psec)	uv	9.14	9.15	8.77	8.93	8.58
$\dfrac{\left(\tau_{rise} + \tau_{fall}\right)}{2}$ *(psec)*	uv	2.36	1.60	2.39	4.10	3.93
Plateau Duration (psec)	uv	6.31	7.23	5.90	4.01	3.86
Bandwidth (nm)	ir	9.8*	9.8*	9.8*	9.8*	9.8*
	blue	4.5	4.3	4.2	3.5	3.4
	uv	3.0	3.0	2.9	2.9	2.8
Plateau Intensity Variation (rms - % of peak)	uv	2.9	2.3	3.5	0.8	1.2
Net Conversion Efficiency (%)	ir	49.7	43.7	42.6	41.8	40.8
	blue	30.1	36.0	33.9	38.0	36.0
	uv	1.3	1.3	4.5	1.2	4.2

* double peaked structure on ir spectra
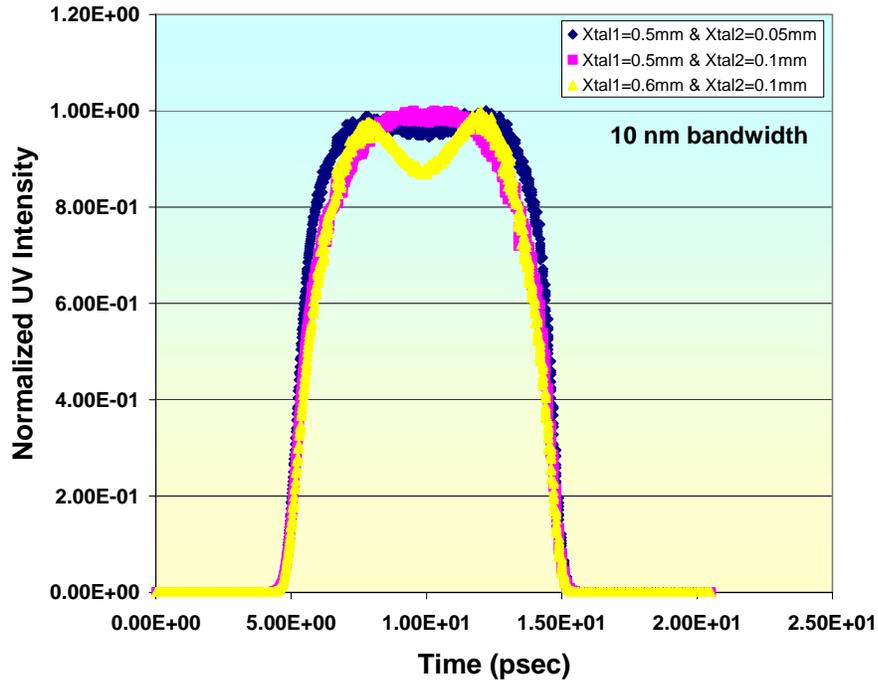
Figure 5. Normalized longitudinal uv intensity profiles at the exit of the second (THG) BBO crystal for the 10 nm incident ir case and various crystal thicknesses.

Table I shows that the uv plateau duration decreases significantly with increasing crystal thicknesses where the maximum is 7.23 psec (for first and second crystal thicknesses of 0.5 and 0.05 mm respectively) and the minimum is 3.86 psec (for first and second crystal thicknesses of 0.6 and 0.1 mm respectively). Finally, the spectral bandwidths of the exiting frequency components corroborate the bandwidth limitation imposed by the crystal thickness. Increasing crystal thicknesses further reduces the bandwidth of the second and third harmonics below the ideal (broadband maximum) values of 5 and 3.3 nm respectively (for the incident ir bandwidth of 10 nm). Therefore, the thinnest case (a 0.4 mm first crystal with a 0.05 mm second crystal) yields the largest second and third harmonic bandwidths of 4.5 and 3.0 nm which are within10% of these ideal values.

III (b) - 5 nm Incident ir Case:

Typical normalized longitudinal intensity profiles for the fundamental and second harmonic that exit the first BBO crystal are shown in figure 6 (plotted results are shown for a BBO thickness of 0.6 mm). The lower incident ir bandwidth of 5 nm is significantly less than the 15 nm intrinsic acceptance value for SHG determined for the 0.6 mm thickness. For the 5nm case, we then anticipate in figure 6 a broader central dip in the ir profile and a similarly broader central peak in the second harmonic profile (relative to the 10 nm case). As with the 10 nm case, the distinction between these two profiles is enhanced with increasing BBO thickness beyond 0.6 mm.
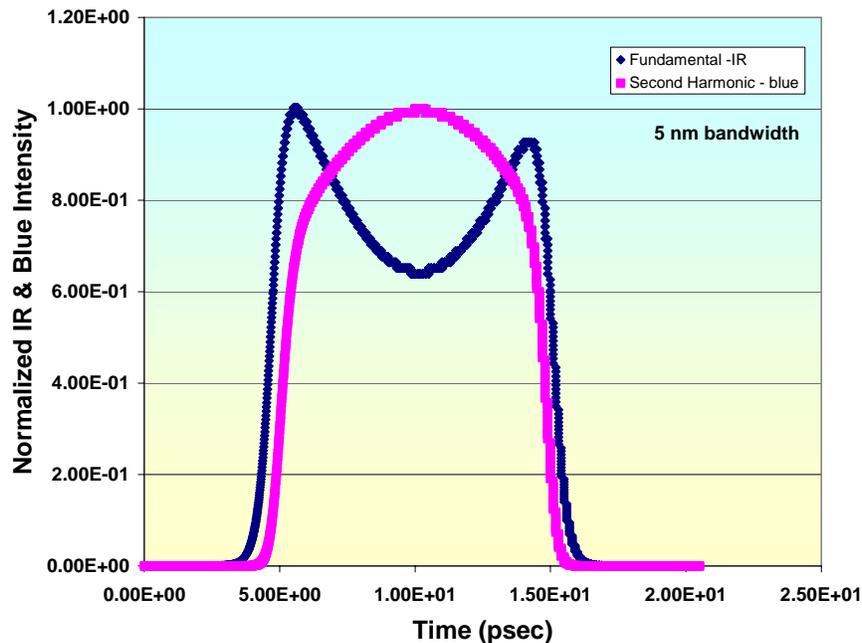
Figure 6. Normalized longitudinal intensity profiles of the fundamental and second harmonic pulses at the exit of the first (SHG) BBO crystal of 0.6 mm thickness for the 5 nm incident ir case

Table II lists best case results for the 5 nm bandwidth case with the same format and definitions as described for Table I. For the 5 nm bandwidth the net SHG efficiency is higher than for the 10 nm case. For example, in the case of a 0.5mm first crystal and a 0.1 mm second crystal the SHG efficiency is increased by about 20% over the 10 nm value. For the case of a 0.6 mm first crystal and a 0.1 mm second crystal this enhancement is about 32%.

Normalized uv profiles for the three best Table II cases are plotted in figure 7. The highest THG efficiency has increased to 20.1 % for the first crystal thickness of 0.7 mm and the second of 0.3 mm. A more rectangular profile is obtained for the slightly thinner case where the first crystal thickness is 0.6 mm and the second is 0.2

mm. However this improvement occurs at the cost of reducing THG efficiency to 14.7 %. Also, we can directly assess the incident ir bandwidth effect by regarding the 0.5 mm first crystal plus 0.1 mm second crystal combination. THG efficiency is 4.5 % and 5.0% for the 10 nm and 5 nm cases respectively. In general, the reduction from an incident bandwidth of 10 nm to 5 nm allows thicker crystals to be used therefore yielding higher THG efficiencies. With this crystal thickness combination as an example, it is clear from Tables I and II that this bandwidth reduction yields major improvements in the uv longitudinal profile with a plateau whose duration is much greater and whose intensity variation is much lower in the 5 nm case.

As was observed also for the 10 nm incident bandwidth, the central dip shown in the longitudinal uv intensity profile for the first and second crystal thickness combination of 0.7mm with 0.3 mm respectively of figure 7 is due to the increased SHG efficiency of the thicker first crystal. Further increase in the second crystal thickness for this case would fill in the dip while also increasing risetime and falltime, reducing acceptance bandwidth and plateau duration, and likely reducing the THG efficiency. In Table II, the maximum listed rms intensity variation in the plateau is only 2.8 % (for the first and second crystal thickness combination of 0.6 mm and 0.2 mm respectively). Note that for the first and second crystal thickness combination of 0.5 mm and 0.1 mm respectively, the rms intensity variation in the plateau is only 1.8 % which about half of that for the same crystal thicknesses using the 10 nm incident bandwidth.

The uv plateau durations ranges from 4.53 to 8.25 psec where higher values are obtained for thinner first crystals. These are also larger values than those obtained for the incident 10 nm case for given crystal thicknesses.

In contrast to the 10 nm bandwidth case, the spectral bandwidth of the second and third harmonics remain within 10 % of the ideal broadband maximum values of 2.5 and 1.7 nm respectively for the listed crystal thicknesses in the 5 nm bandwidth case (with the exception of the third harmonic bandwidth in the thickest case of a 0.7mm first crystal with a 0.3 mm second crystal which is within about 16 %). Also, as with the 10 nm case, the intrinsic acceptance bandwidth for the second crystal is comparable to the incident ir value for the thickest cases listed (i.e. 5.0 nm for 0.2 mm and 3.3 nm for 0.3 mm).

Finally, where the THG efficiency is low, we can expect the longitudinal intensity profiles of the fundamental and second harmonic light at the exit of the second crystal to resemble those that are incident on it (as indicated in figure 6).

Table II: 5nm bandwidth Case

		0.5	0.6	0.6	0.7	0.7
Crystal 1 depth (mm)		0.5	0.6	0.6	0.7	0.7
Crystal 2 depth (mm)		0.1	0.1	0.2	0.2	0.3

FWHM *(psec)*	uv	9.50	9.55	9.35	9.37	8.80
$\dfrac{(\tau_{rise} + \tau_{fall})}{2}$ *(psec)*	uv	1.04	3.73	1.59	4.03	2.14
Plateau Duration (psec)	uv	8.25	5.07	7.44	4.53	6.23
Bandwidth (nm)	ir	4.9*	4.9*	5.1*	5.1*	5.1*
	blue	2.3	2.2	2.2	2.2	2.2
	uv	1.5	1.5	1.5	1.5	1.4
Plateau Intensity Variation (rms - % of peak)	uv	1.8	0.7	2.8	0.5	2.7
Net Conversion *Efficiency (%)*	ir	35.4	28.8	25.4	22.4	19.9
	blue	40.6	47.4	40.6	44.9	39.9
	uv	5.0	4.6	14.7	13.3	20.1

* double peaked structure on ir spectra
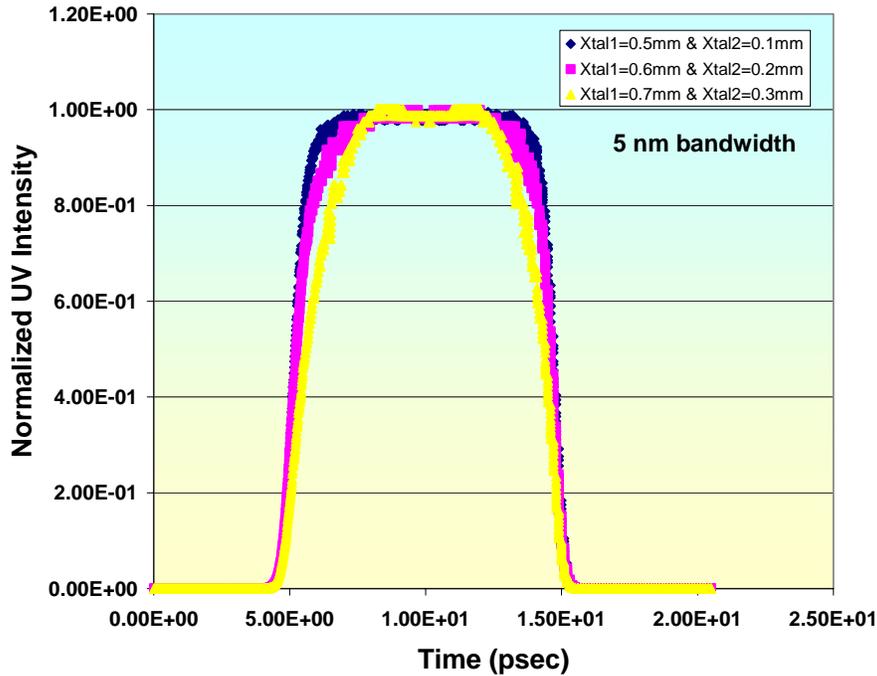
Figure 7. Normalized longitudinal uv intensity profiles at the exit of the second (THG) BBO crystal for the 5 nm incident ir case and various crystal thicknesses.

III (c) - 2.5 nm Incident ir Case

As the lowest bandwidth case addressed here, the 2.5 nm is approximately equal to the Fourier transform limit required at the ir wavelength for realistic longitudinal pulse profiles [6]. Figure 8 shows typical normalized longitudinal profiles for ir and second harmonic light that exit the first BBO crystal and are also incident on the second one (plotted results are for a first BBO crystal thickness of 0.7 mm). The 2.5 nm incident ir bandwidth is significantly lower than the 12.9 nm estimate for intrinsic acceptance bandwidth based on a 0.7 mm first crystal thickness. Consequently, the central dip in the ir profile is noticeably broader than that illustrated in figures 4 and 6, and the second harmonic profile begins to appear quasi-rectangular. As the first crystal thickness is increased beyond 0.7 mm, its intrinsic acceptance bandwidth is reduced and the two profiles become more distinct with the ir central dip becoming deeper and the second harmonic profile becoming more centrally peaked and less rectangular (more centrally peaked as in the case of figure 4). Table III lists best case results for the 2.5 nm case with the format and definitions being the same as in Tables I and II. With the exception of the first and second crystal thickness combination of 0.4 and 0.2 mm respectively, the net SHG efficiency remains above 35%.
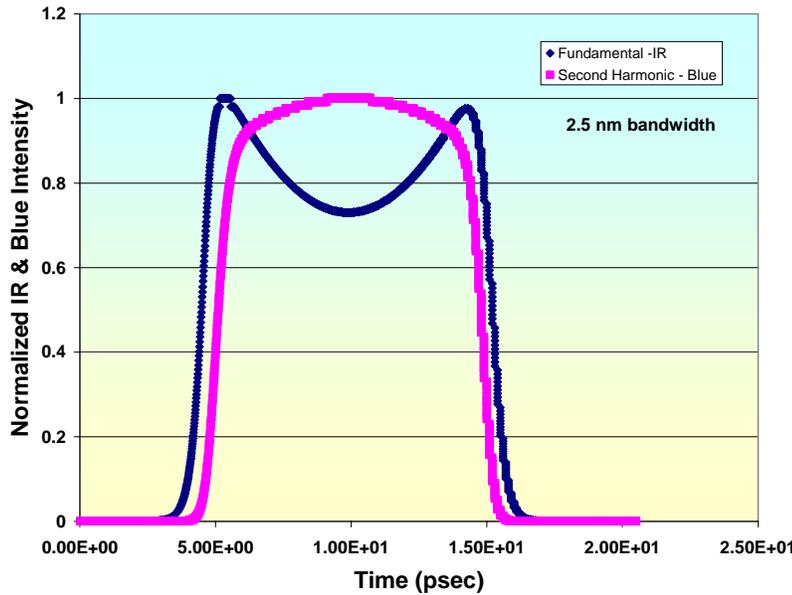
Figure 8. Normalized longitudinal intensity profiles of the fundamental
and second harmonic pulses at the exit of the first (SHG) BBO
crystal of 0.7 mm thickness for the 2.5 nm incident ir case

Figure 9 illustrates normalized longitudinal profiles for the best three uv cases of Table III. The figure again reveals the small central dip in the uv profile that is due to the increased SHG efficiency in the first crystal. Further increase of the second crystal thickness beyond 0.5 mm will fill in this dip at the cost of reduced acceptance bandwidth, increased risetime and falltime, as well as reduced plateau duration and THG efficiency. In Table III, the maximum listed rms intensity variation in the plateau is only 3.2 % (for the first and second crystal thickness combination of 0.6 mm and 0.3 mm respectively). Note that   for the first and second crystal thickness combination of 0.6 mm and 0.2 mm respectively, the rms intensity variation in the plateau is only 1.6 % which is near half of that for the same crystal thicknesses using the 5 nm incident bandwidth.

The THG efficiencies are expectedly higher than for the 5 and 10 nm bandwidth cases and ranging from 15.7 to 28.9 % (where the highest efficiency is achieved for the first and second crystal thickness combination of 0.8 and 0.5 mm respectively). Also, these results are obtained for crystal thicknesses that are higher than those used for the broader ir bandwidths. Figure 9 also indicates that the quasi-rectangular profile shape is noticeably improved by reducing the first and second crystal thickness to 0.7 and 0.3 mm respectively. This is done at the cost of a THG efficiency reduction to 23.9 %. Regarding the first and second crystal thickness combinations of 0.6 with 0.2 mm as well as 0.7 with 0.3 mm respectively, comparison of Tables II and III indicates that the THG efficiency is slightly improved at the lower bandwidth.

Plateau durations are higher than those for the broader ir bandwidths. They range from 7.23 to 8.56 psec. This is mainly due to the reduced risetime and falltime values. Again we compare the first and second crystal thickness combinations of 0.6 mm with 0.2 mm and 0.7 mm with 0.3 mm for the 5.0 nm and 2.5 nm cases. For the 2.5 nm case, the uv plateau durations are larger because the risetime and falltime are significantly reduced (to 0.92 psec and 0.94 psec for the two thickness combinations). It is clear that the combined THG efficiency and rectangular shape requirements are best met with this lowest bandwidth case.

For comparison, it is worth noting that the risetime and falltime, the FWHM (and therefore the plateau duration) and the rms intensity modulation on the plateau have been examined for the Fourier transform limited case with this nominal incident ir longitudinal profile and in the absence of harmonic generation processes [6]. Based on this previous work we estimate a transform limited plateau duration of at least 8.8 psec with a plateau intensity (rms) variation less than 1.0 % for the 2.5 nm bandwidth without harmonic generation effects. Table III results approach this combination of values.

The second and third harmonic bandwidths of 1.1 and 0.7 nm respectively are within 10 % of the ideal broadband maximum values (which are 1.25 and 0.8 nm respectively) for all listed thicknesses. This is similar to the bandwidth results for the 5 nm case. For a second BBO crystal thickness of 0.3 to 0.5 mm the intrinsic acceptance bandwidth is 3.3 to 2.0 nm which brackets the 2.5 incident ir value. This general result concerning the maximum second crystal thickness is similar for all three bandwidth cases.

<div align="center">Table III: 2.5 nm bandwidth Case</div>

Crystal 1 depth (mm)		0.4	0.6	0.6	0.7	0.8
Crystal 2 depth (mm)		0.2	0.2	0.3	0.3	0.5
FWHM (psec)	uv	9.40	9.63	9.50	9.69	9.46
$\dfrac{(\tau_{rise} + \tau_{fall})}{2}$ *(psec)*	uv	1.15	0.92	1.40	0.94	1.88
Plateau Duration (psec)	uv	8.02	8.53	7.82	8.56	7.20
Bandwidth (nm)	ir	2.3*	2.3*	2.3*	2.6*	2.6*
	blue	1.1	1.1	1.1	1.1	1.1
	Uv	0.7	0.7	0.7	0.7	0.7
Plateau Intensity Variation (rms - % of peak)	uv	2.5	1.6	3.2	1.4	3.0
Net	ir	39.8	21.2	17.0	12.4	7.0
Conversion	blue	23.6	44.0	35.5	44.4	44.4
Efficiency (%)	uv	17.7	15.7	28.2	23.9	28.9

* double peaked structure on ir spectra
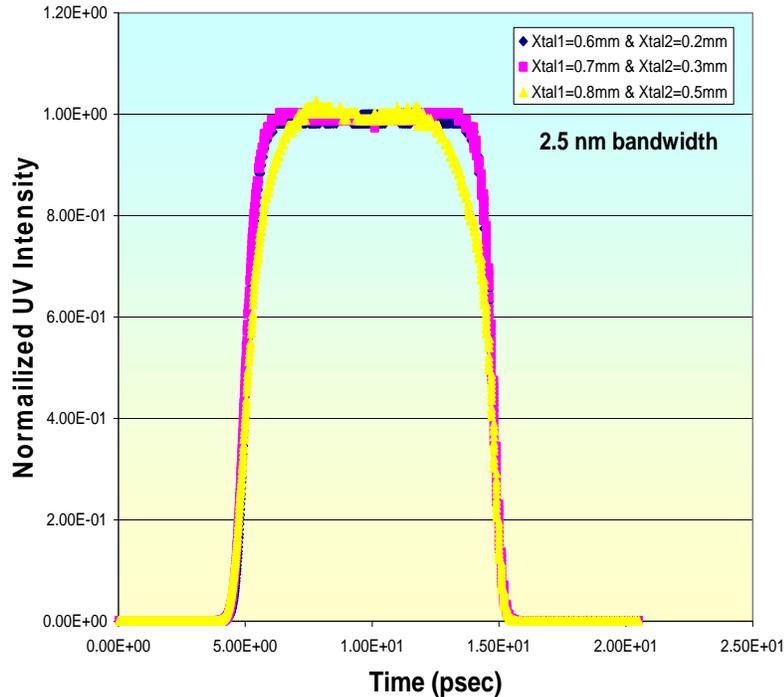
Figure 9. Normalized longitudinal uv intensity profiles at the exit of the second (THG) BBO crystal for the 2.5 nm incident ir case and various crystal thicknesses.

IV. Summary

A few general comments can be made about what is presented in the three tables. Lower incident ir bandwidths allow use of thinner crystals to obtain a specified THG efficiency which means that for fixed crystal thicknesses, the lower bandwidth typically yields a higher THG efficiency. More importantly, the lower bandwidth yields significantly higher THG efficiency when constrained only by longitudinal pulse shape requirement for a quasi-rectangular, flattop pulse. Furthermore, because the second crystal intrinsic acceptance bandwidths approximately match the incident ir values, it is the second crystal thickness that limits these THG efficiency and longitudinal profile results. These results indicate the merits of minimizing the incident ir bandwidth for obtaining, with adequate efficiency, third harmonic pulses of quasi-rectangular longitudinal profile. Of the three incident ir bandwidth cases investigated, 5 nm appears to be a suitable compromise value in the context of widely available broadband ir laser systems. Relay imaging and other propagation issues such as group velocity dispersion will also benefit from the use of minimal bandwidth.

We have shown the utility of the SNLO code, as modified for the plane wave case, in addressing coupled cases such as this. The 2D case that includes the effects of beam focusing can be addressed when similar modifications are made available. Results

reported here provide reference data for development and design of 'shaped' second and third harmonic longitudinal profiles. Furthermore, these results are exclusively SNLO predictions and controlled comparisons with experimental data must be made.

It is clear that incident ir pulses of duration longer than 10 psec (for any given bandwidth addressed in this work) are expected to see improved SHG and THG phase matching over a nominal 10 psec interval because the relevant bandwidth is reduced over this time interval. However, temporal pulse stretching reduces the peak intensities and therefore the efficiency for SHG and THG. Furthermore, independent control of longitudinal profiles exists over the stretched time scale (with the central 10 psec profile determined by the phase matching). Incident ir pulses of duration shorter than 10 psec face the same bandwidth limits as the 10 psec pulses within the shorter duration and the increased peak ir intensity can improve the THG efficiency for lower crystal thicknesses.

In addition to the 2D investigation, another important extension of this work is to examine quasi-rectangular longitudinal profiles with nonzero plateau slopes (the uv pulse specification for the LCLS injector includes slope variation of -10% to +20 %) and with plateau intensity noise (the uv pulse specification for the LCLS injector includes a maximum 5% rms plateau intensity variation). We are currently investigating these features that will be the subject of a subsequent report. Other natural extensions include investigating the effects of sequestering a portion of the incident ir for THG alone (i.e. bypassing the first crystal), examination of shorter incident pulse durations (the uv pulse specification for the LCLS injector includes duration adjustment from 5 to 20 psec), testing other phase matching schemes, and possibly including the effects of shaping incident ir transverse profiles.

Acknowledgements:

References:

1.   SNLO nonlinear optics code available from A.V. Smith, Sandia National Laboratories, Albuquerque, NM 87185-1423.
2.   P.R. Bolton and B.F. Murphy, LCLS-TN-02-1 (Dec.'01)
                    and SLAC-TN-05-031 (Dec.'01)
3.   B.C. Stuart et al., Phys. Rev. B53, 1749 ('96).

4.   A.V. Smith, private communication.

5.   A. Yariv "Quantum Electronics" Second Edition, Chapter 16 (pp 424), John Wiley & Sons, Inc., 1975.
6.   C. Limborg-DePrey and P.R. Bolton, LCLS-TN-04-16 (Nov.'04)
                    and SLAC-TN-05-012 (Nov.'04)